Collective transport properties of skyrmions on the depinning phase transition

L. Xiong,[1,2] B. Zheng,[1,2,*] M. H. Jin,[1,2] and N. J. Zhou[3]

[1]Department of Physics, Zhejiang University, Hangzhou 310027, People's Republic of China

[2]Collaborative Innovation Center of Advanced Microstructures, Nanjing University, Nanjing 210093, People's Republic of China

[3]Department of Physics, Hangzhou Normal University, Hangzhou 310036, People's Republic of China

(Received 17 March 2019; revised manuscript received 12 August 2019; published 27 August 2019)

The pinning phenomena of topological skyrmions in magnetic materials with defects are of vital importance for the precise positioning and the manipulation of skyrmions in experiment. With the Thiele equation of the particle-based model, we investigate the dynamic depinning phase transition of skyrmions, induced by quenched disorder. The phase transition from the pinned glass to the moving liquid is of second order, while the critical driving force and both the static and dynamic exponents are accurately determined for different strengths of the Magnus term and the pinning force based on the dynamic scaling behavior far from stationary. The results show that the skyrmions exhibit very different collective transport properties at the depinning phase transition due to the Magnus force which induces the skyrmion Hall effect compared to the overdamped magnetic systems. Furthermore, the critical behaviors of skyrmions are anisotropic in directions perpendicular and parallel to the driving force, providing an understanding of the force-dependent Hall angle around the phase transition in experiment. Our nonstationary dynamic approach is very efficient in tackling the dynamic phase transitions.

DOI: 10.1103/PhysRevB.100.064426

I. INTRODUCTION

Skyrmions are topologically stable field configurations with particlelike properties, originally proposed to describe the resonance states of baryons in nuclear physics [1]. Such topological states have been observed experimentally in ferromagnetic metals such as MnSi and FeGe [2–5]. The experiments suggest that the periodic skyrmion crystal configurations can be stabilized by Dzyaloshinskii-Moriya interactions or dipole-dipole interactions in ferromagnets at room temperature [2,6–8]. As the topological textures are similar to those of domain walls, skyrmions can also be driven by an electric current. Further, it has been experimentally demonstrated that an ultralow current density, which is orders of magnitude smaller than that typically used for domain-wall manipulation, may drive translational and rotational motions of skyrmions [7,9–12]. Compared to domain walls, skyrmions could have enormous advantages as information carriers, such as low energy cost and low Joule heating. Thus, the manipulation of skyrmions is an important topic.

The hexagonal crystal state of skyrmions in chiral magnets has been measured in neutron scattering experiments and in direct imaging experiments in thin films [2,13]. In the presence of quenched disorder, the skyrmion-crystal dynamics is vastly different. For weak disorder, the skyrmions may mostly retain the hexagonal order, while strong disorder would cause a proliferation of topological defects and push the skyrmions into an amorphous state or a glassy one. When an external driving force greater than the critical value is applied, the skyrmions transform from the glassy state to the fluid one and further reorder into a moving skyrmions crystal under a high driving force [14]. The current-driven motion of skyrmions has been directly imaged in experiments. Through experimental transport measurements, it is possible to obtain the skyrmion-crystal velocity versus the applied driving force and to detect a finite-depinning threshold [3,5,10,15–17]. Theoretical investigations have also indicated that there is a depinning phase transition of skyrmions in the ferromagnetic material with quench disorder [12,14,18–20].

The description of skyrmions is mostly based on continuum models with high computational complexity. Thiele analyzed the Landau-Lifshitz-Gilbert equation and derived the so-called Thiele equation for describing the dynamic behavior of various magnetic textures in magnetic materials [21]. Previous studies showed that the Thiele equation of the particle-based model, which summarizes the skyrmion-skyrmion interaction and the skyrmion-defect interaction, agrees well with the Landau-Lifshitz-Gilbert equation for the dynamic properties of skyrmions in magnetic materials in the presence or absence of defects, such as the pinning effect, the rotation of a skyrmion crystal due to the temperature gradient, etc. [6,12,22,23].

Numerical simulations highlighted the static and dynamic phases for skyrmions through the particle-based simulations in Ref. [14]. In the presence of defects, the skyrmions undergo a dynamic depinning phase transition from a pinned skyrmion glass to a disordered flowing state. With higher driving forces, there is an additional phase transition from the disordered flowing state reordering into a moving crystal [14]. We focus on only the depinning phase transition in this paper. Similar to vortices in type-II superconductors, skyrmions exhibit a particlelike nature and can be externally driven by an electric current. The vortex dynamics is usually assumed to be overdamped, and the Magnus force is negligibly small. In contrast, the damping effect in the skyrmion motion is relatively weak,

*zhengbo@zju.edu.cn

and the Magnus force is dominant. Hence, skyrmions extraordinarily drift along the perpendicular direction of the driving force due to the Hall effect [15,24–27] and are more easily deflected by pinning centers. In fact, a recent experiment suggests that the skyrmion Hall angle depends on the driving force in the presence of defects at low driving force. The Hall angle is zero in the pinning state and exhibits a roughly linear dependence on the increasing drive until it reaches its saturation value [15]. Moreover, the velocities of the vortices in the directions perpendicular and parallel to the driving force are independent, while those of the skyrmions are conjugated [6]. However, the experiment indicates that the velocities of skyrmions in both directions may be unrelated around the depinning phase transition. It reveals that there may be different dynamic behaviors in the directions perpendicular and parallel to the driving force on the depinning phase transition, but an elaborate study is absent. Thus, the Magnus interaction would induce novel collective transport behavior in the depinning phase transition of skyrmions with defects.

There have been theoretical studies on depinning phase transitions of domain walls and vortices, etc. [28–33], which together with skyrmions are usually considered to be topological excitations in magnetic materials. In addition, due to the prominent nondissipative interaction, the critical dynamics of skyrmions is very different from other collectively driven systems with random disorder. The critical behavior of skyrmions has scarcely been investigated [34]. Important properties of the phase transition, including its order and universality class, are still unclear. Due to critical slowing down, it is extremely difficult to simulate the stationary state close to the phase transition point. The nonstationary dynamic approach looks novel and efficient in tackling the dynamic phase transitions of domain walls since the measurements are carried out in the short-time regime of the dynamic evolution [35,36]. Such a dynamic approach is methodologically even more important for the complex skyrmion system governed by the Thiele equation of the particle-based model or the Landau-Lifshitz-Gilbert equation. In addition, it may avoid the errors induced by the finite time step Δt in the molecular dynamics simulations of the stationary state.

In this paper, numerical simulations based on the Thiele equation of a particle model are performed for the nonstationary dynamic relaxation of skyrmions in a magnetic thin film with quench disorder. We choose model parameters approaching the typical experimental material MnSi [2,6,22]. It is demonstrated that the phase transition point and both the static and dynamic critical exponents can be accurately determined with the refined nonstationary dynamic approach. The critical dynamic behaviors of the depinning phase transitions of skyrmions, domain walls, and vortices are also compared. In Sec. II, the model is described, and in Sec. III, the dynamic scaling analysis is presented. In Sec. IV, numerical simulations are performed. Finally, Sec. V includes the conclusions.

II. EQUATION OF MOTION

We simulate interacting skyrmions with random disorder based on a recently developed particle model [22], where the skyrmion size and the average distance of skyrmions are comparable. The skyrmions are regarded as particles in the x-y plane, and the dynamic evolution of a skyrmion i at $\mathbf{r}_i$ is governed by the modified Thiele equation [22]:

$$\alpha_d \mathbf{v}_i + \alpha_m \hat{z} \times \mathbf{v}_i = \mathbf{F}_i^{ss} + \mathbf{F}_i^{sp} + \mathbf{F}, \tag{1}$$

where $\mathbf{v}_i = d\mathbf{r}_i/dt$ is the skyrmion velocity. The damping term with the coefficient α_d aligns the skyrmion velocity with the net force acting on the skyrmion, while the Magnus term with the coefficient α_m represents the Hall effect and causes the skyrmion to drift in the perpendicular direction. We impose the constraint $\alpha_d^2 + \alpha_m^2 = 1$ to maintain a constant magnitude of the skyrmion velocity as α_m/α_d varies. For experimental systems such as MnSi, one observes $\alpha_m/\alpha_d \approx 10$. In this work, we first focus on $\alpha_m/\alpha_d = 9.962$, which is also considered in Ref. [14] and corresponds to the Magnus-dominated dynamics [10,13,22], and then extend the simulations to other strengths of the Magnus forces.

The skyrmion-skyrmion interaction is $\mathbf{F}_i^{ss} = \sum_{j=1}^{N_s} K_1(R_{ij})\hat{\mathbf{r}}_{ij}$, where $R_{ij} = |\mathbf{r}_i - \mathbf{r}_j|$, $\hat{\mathbf{r}}_{ij} = (\mathbf{r}_i - \mathbf{r}_j)/R_{ij}$, and $K_1(R)$ is the modified Bessel function. The interactions between skyrmions and quenched defects are taken to be $\mathbf{F}_i^{sp} = \sum_{j=1}^{N_d} F_{\text{pin}} \exp(-R_{ij})\hat{\mathbf{r}}_{ij}$, and F_{pin} is the strength of the pinning force [23]. The pinning centers of defects are randomly distributed in the simulation box, with nonoverlapping harmonic traps of the size $R_p = 0.3$; that is, the distance between any two pinning centers is not less than 0.3. $\mathbf{F}$ is the external driving force along the x direction.

For comparison to the experiment, dimensions of the model parameters should be attended. The parameters of the model are derived from those typical of MnSi [14,22]. In the MnSi thin film, the lattice constant $a \approx 3$ Å, the exchange energy $J \approx 3$ meV$/a$, and the Dzyaloshinskii-Moriya energy $D \approx 0.3$ meV$/a^2$. The skyrmion size is $\xi = 2\pi J/D \approx 19$ nm. The repulsive force F^{ss} between two skyrmions is in units of 10^{-5} N/m [22]. For the external current $j \sim 10^8$ A/m^2; the corresponding driving force is $F = 2\pi\hbar e^{-1} j \sim 4 \times 10^{-7}$ N/m.

In our simulations, the size of the simulation box is $L_x \times L_y$, with periodic boundary conditions in both directions. In order to simulate the collective dynamic transport behaviors around the pining-depinning phase transition, we initialize the skyrmions to a hexagonal skyrmion crystal in the x-y plane, which is the spontaneous skyrmion ground state without disorder, and investigate the dynamic relaxation process in the macroscopic short-time regime. In principle, other initial states with a minimal spatial correlation length, which would not induce strong corrections to scaling, can be also adopted. We take the perfect hexagonal configuration as the initial state, mainly for simplicity. Our simulations confirm that other initial states yield the same critical dynamic behaviors.

The number of skyrmions is typically $N_s = 80 \times 80$. The skyrmion density $\rho_s = N_s/(L_x L_y)$ is set to 0.1, and it implies a grid size $l_s = (\rho_s\sqrt{3}/2)^{-1/2}$. In order to achieve the density of skyrmions, $\rho_s = 0.1$, the simulation box is taken to be $L_x = l_s\sqrt{N_s}$ and $L_y = l_s\sqrt{3N_s}/2$. The number of defects, $N_d = L_x L_y \rho_d$, is fixed by $\rho_d = 0.3$, and the cutoff radius is set to be $r_c = 6.0$. The time step $\Delta t = 0.05$ is used in the molecular dynamics simulation of the Thiele equation. In our setting of the parameters, the time t is dimensionless. The maximum simulation time is $t_{max} = 10\,000$ in each sample, and the number of total samples of quenched disorder on average is about 10 000.

III. THEORETICAL ANALYSIS

Keeping in mind that the driving force **F** is in the x direction, we define the average velocity in the perpendicular direction as

$$V_\perp(t) = \frac{1}{N_s}\sum_{i=1}^{N_s}\langle v_i^y(t)\rangle, \tag{2}$$

where $v_i^y(t)$ is the y component of the velocity of skyrmion i and $\langle\cdots\rangle$ represents the statistical average over the samples of different random defects. The average velocity in the parallel direction of the driving force denoted by $V_\parallel(t)$ is defined in the same way, with the velocity component in the x direction. Under a strong pinning force and with the initial state of a hexagonal crystal, the skyrmions driven by the external force will collectively move around the crystal structure and gradually evolve to a glassy state or a liquid one.

In the stationary state, the skyrmion motion driven by a constant external force exhibits a depinning phase transition. The phase transition force F_c separates the pinned amorphous glass state and the moving liquid state of the skyrmions, where the collective velocities are zero and nonzero, respectively. Assuming the depinning phase transition is second order, there should exist a dynamic scaling form in the macroscopic short-time regime based on the renormalization group arguments after a microscopic timescale t_{mic} [37,38]. In the critical regime and for a sufficiently large simulation box, the dynamic scaling form of the order parameter, i.e., the average velocity of the skyrmions in the perpendicular direction, is described as

$$V_\perp(t,\tau) = t^{-\beta_\perp/\nu_\perp z_\perp}G(t^{1/\nu_\perp z_\perp}\tau), \tag{3}$$

where $\tau = (F - F_c)/F_c$ is the reduced force, $\beta_\perp$ and $\nu_\perp$ are static critical exponents, and $z_\perp$ is the dynamic critical exponent. At the critical force, $\tau = 0$, it leads to a power-law behavior,

$$V_\perp(t) \sim t^{-\beta_\perp/\nu_\perp z_\perp}. \tag{4}$$

Therefore, searching for the best power-law behavior of $V_\perp(t,\tau)$, one may locate the transition force F_c and then measure the exponent $\beta_\perp/\nu_\perp z_\perp$. The exponent $1/\nu_\perp z_\perp$ can be extracted from the logarithmic derivative of Eq. (3),

$$\left.\frac{\partial \ln V_\perp(t,\tau)}{\partial\tau}\right|_{\tau=0} \sim t^{1/\nu_\perp z_\perp}. \tag{5}$$

Further, the Binder cumulant of the velocity is defined as

$$v_\perp^{(2)}(t) = \frac{\langle\left[\sum_{i=1}^{N_s} v_i^y(t)/N_s\right]^2\rangle - V_\perp(t)^2}{V_\perp(t)^2}. \tag{6}$$

We also measure the autocorrelation function of the velocity

$$A_\perp(t,t_0) = \left\langle\sum_{i=1}^{N_s} v_i^y(t)v_i^y(t_0)\right\rangle, \tag{7}$$

where t_0 is the waiting time and $t_0 < t$. At the critical force, based on the finite-size scaling analysis and assuming the nonstationary spatial correlation length $\xi_\perp(t)$ is small, the Binder cumulant should scale as

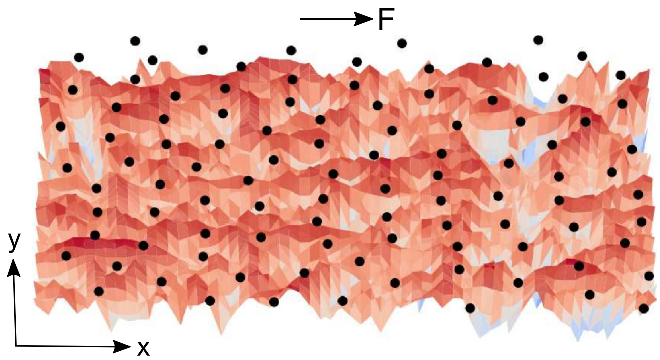

FIG. 1. A schematic snapshot of the driven skyrmions in a two-dimensional pinning landscape induced by disorder. Black dots indicate the skyrmion centers.

$$v_\perp^{(2)}(t) \sim (\xi_\perp(t)/L_y)^d, \tag{8}$$

where $d = 2$ is the spatial dimension. In the scaling regime, $\xi_\perp(t)$ usually grows as a power law, $\xi_\perp(t) \sim t^{1/z_\perp}$. According to Ref. [39], the autocorrelation function may obey the dynamic scaling form

$$A(t,t_0) = \xi(t_0)^{-\eta}F[\xi(t)/\xi(t_0)], \tag{9}$$

where the critical exponent $\eta/2$ is the scaling dimension of the skyrmion velocity and the scaling function $F[\xi(t)/\xi(t_0)]$ represents the temporal scale invariance in the critical regime [39,40].

To estimate the structure information of skyrmions, we measure the mean-square displacement in the center-of-mass frame [41],

$$\Delta r^2(t) = \langle|\mathbf{r}_i(t) - \mathbf{r}_i(0) - [\mathbf{r}_{cm}(t) - \mathbf{r}_{cm}(0)]|^2\rangle, \tag{10}$$

where $\mathbf{r}_i(t)$ is the position of skyrmion i without considering the periodic boundary condition and $\mathbf{r}_{cm}(t) = \sum_{i=1}^{N_s}\mathbf{r}_i(t)/N_s$ is the center of mass of the simulation box at time t. The angle brackets $\langle\cdots\rangle$ represent the average over all skyrmions and samples. In addition, the pair distribution function is also calculated at each time, which is defined as

$$g(r) = \frac{2S}{N_s^2}\left\langle\sum_{i<j}\delta(\mathbf{r} - \mathbf{r}_{ij})\right\rangle, \tag{11}$$

where $\mathbf{r}_{ij}$ is the distance between skyrmions i and j and $g(r)$ describes the relative probability of finding a particle in the volume element Δr at a distance r from a given particle [42].

IV. NUMERICAL SIMULATIONS

A schematic snapshot of the driven skyrmions in the magnetic thin film with quenched disorder is shown in Fig. 1. In the numerical simulations, we first set the Magnus term $\alpha_m/\alpha_d = 9.962$ and the strength of the pinning force $F_{\mathrm{pin}} = 0.03$ and perform the measurements for the average velocities of skyrmions, both perpendicular and parallel to the driving force. In Fig. 2, the velocity $V_\perp(t)$ versus the time t is plotted for different driven forces. The critical force

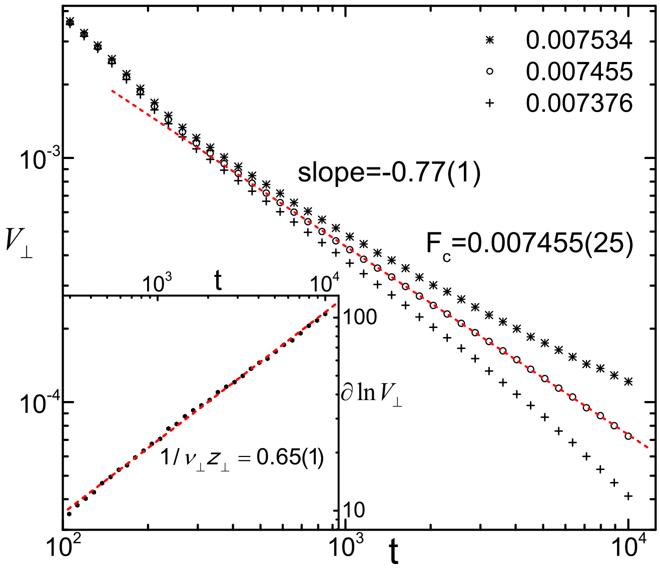

FIG. 2. The perpendicular velocity $V_\perp$ versus the time t for different driving forces with $\alpha_m/\alpha_d = 9.962$ and $F_{\rm pin} = 0.03$ on a log-log scale. A power-law behavior at the critical force $F_c = 0.007455$ is detected. The inset shows the logarithmic derivative of $\partial_\tau \ln V_\perp(t, \tau)$ at F_c. Dashed lines show power-law fits.

$F_c = 0.007455(25)$ is determined through searching for the best power-law behavior in the time regime $t \geqslant t_{\rm mic} \sim 250$. This value of the critical force F_c is equivalent to $j \approx 0.7455 \times 10^6$ A/m^2, which is consistent with the critical current $j_c \sim 10^6$ A/m^2 in the experiment with MnSi [10,13] and the simulation result of Ref. [14] within errors. From the slope of the curve, one measures the critical exponent $\beta_\perp/\nu_\perp z_\perp = 0.77(1)$, according to Eq. (4). In the inset, the logarithmic derivative $\partial_\tau \ln V_\perp(t, \tau)$ at the critical force is displayed. With Eq. (5), the slope of the curve yields the critical exponent $1/\nu_\perp z_\perp = 0.65(1)$.

The dynamic scaling form in Eq. (3) holds under the assumption that there exist no extra relevant spatial length scales besides the divergent one described by $\tau^{-\nu_\perp}$. Otherwise, the power-law behavior at the critical force would be modified by this length scale. In our particle model with the Thiele equation, one does not find the mechanism of such an extra length scale [19,22,43]. Anyway, to further numerically validate our results, we perform the simulation up to a longer time, $t = 30\,000$, with a larger simulation box $N_s = 160 \times 160$ at the critical force F_c, and the power-law behavior remains the same. Simulations for even longer times becomes very difficult with our computer resources due to the high computational complexity induced by the finite-Δt and finite-size effects.

To estimate the nonstationary spatial correlation lengths in both directions, the Binder cumulants of the velocities are calculated. In Fig. 3, the perpendicular correlation length $\xi_\perp(t)$ and the parallel correlation length $\xi_\parallel(t)$ at F_c are shown. The perpendicular correlation length $\xi_\perp(t)$ exhibits an almost perfect power-law behavior, and the slope of the curve gives the dynamic critical exponent $1/z_\perp = 0.55(1)$. For the parallel correlation length $\xi_\parallel(t)$, however, there exists a strong correction. Fitting the curve with a power-law correction, i.e., $\xi_\parallel(t) \sim t^{1/z}(1 + c/t)$, it yields the dynamic exponent $1/z_\parallel = 0.78(2)$.

Since the skyrmion system is Magnus dominated, there is a typical Hall effect when the skyrmions are driven by an external force. The Magnus term induces a transverse deflection for the skyrmion motion relative to the direction of the external driving force. Due to this Hall effect, the skyrmion motion is different in the parallel and perpendicular directions.

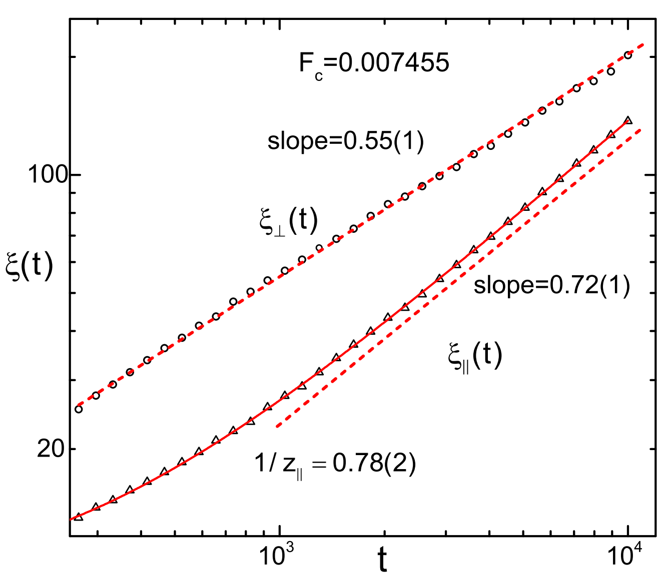

FIG. 3. The spatial correlation lengths in both directions, $\xi_\perp(t)$ and $\xi_\parallel(t)$, at F_c with $\alpha_m/\alpha_d = 9.962$ and $F_{\rm pin} = 0.03$ are plotted. Dashed lines show power-law fits, and the solid line represents a power-law fit with a power-law correction.

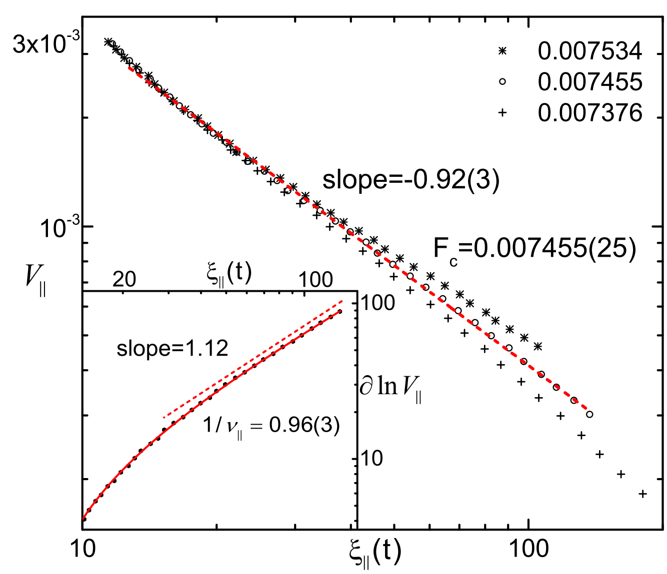

FIG. 4. The parallel velocity $V_\parallel$ versus the spatial correlation length $\xi_\parallel(t)$ for different driving forces with $\alpha_m/\alpha_d = 9.962$ and $F_{\rm pin} = 0.03$ on a log-log scale. In the inset, the logarithmic derivative of $\partial_\tau \ln V_\parallel(t, \tau)$ at the critical force F_c is plotted. Dashed lines show power-law fits, and the solid line represents a power-law fit with a power-law correction.

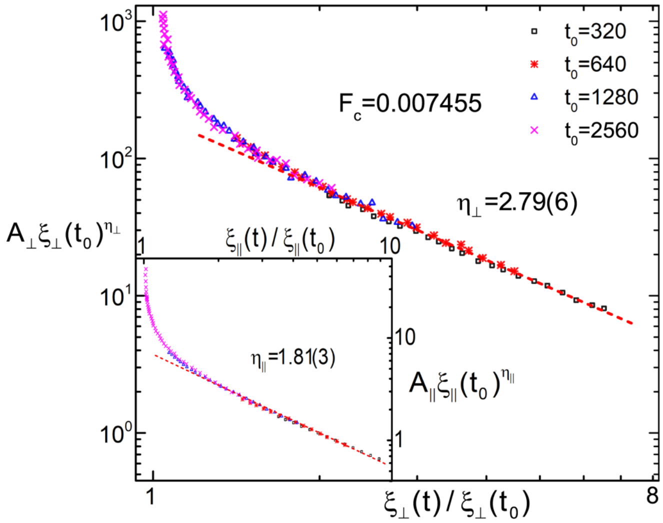

FIG. 5. Data collapse of the autocorrelation function $A_\perp(t, t_0)$ of the perpendicular velocity with $\alpha_m/\alpha_d = 9.962$ and $F_{\rm pin} = 0.03$ is displayed, and $A_\parallel(t, t_0)$ is shown in the inset. Dashed lines show power-law fits.

A similar scaling analysis was applied to $V_\parallel$, but a visible deviation from the power-law behavior at the critical force $F_c = 0.007455$ is observed, in contrast to $V_\perp$. Our conjecture is that this deviation may be induced by the correction to scaling of the spatial correlation length $\xi_\parallel(t)$. Hence, $\xi_\parallel(t)$ rather than t is taken as the dynamic scaling variable. The dynamic scaling form of the average velocity $V_\parallel$ is rewritten as

$$V_\parallel(t, \tau) = \xi_\parallel(t)^{-\beta_\parallel/\nu_\parallel} G(\xi_\parallel(t)^{1/\nu_\parallel}\tau). \tag{12}$$

Thus, $V_\parallel$ and the logarithmic derivative $\partial_\tau \ln V_\parallel$ at the critical force are scaled as $\xi_\parallel(t)^{-\beta_\parallel/\nu_\parallel}$ and $\xi_\parallel(t)^{1/\nu_\parallel}$, respectively. In Fig. 4, the average velocity $V_\parallel$ versus $\xi_\parallel(t)$ is displayed for different driven forces. One obtains the critical exponent $\beta_\parallel/\nu_\parallel = 0.92(3)$ by measuring the slope of the curve at the critical force $F_c = 0.007455$. In the inset, the logarithmic derivative $\partial_\tau \ln V_\parallel$ at F_c is plotted, and the slope of the curve gives the critical exponent $1/\nu_\parallel = 0.96(3)$.

With the dynamic scaling form in Eq. (9), the data collapse of the autocorrelation function $A_\perp(t, t_0)$ of the perpendicular velocity for different t_0 at the critical force F_c is shown in Fig. 5, and one extracts the critical exponent $\eta_\perp = 2.79(6)$.

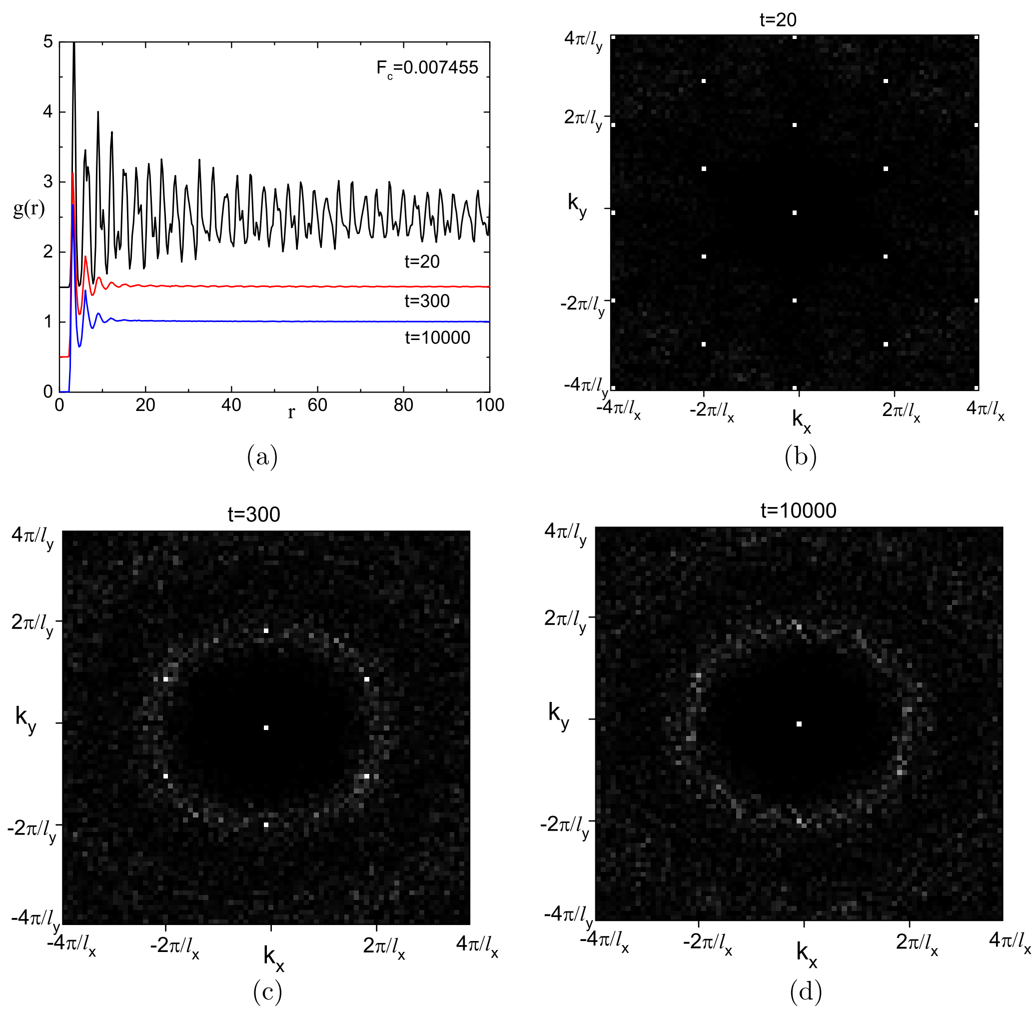

FIG. 6. (a) The pair distribution function at the critical force $F_c = 0.007455$ for different times with $\alpha_m/\alpha_d = 9.962$ and $F_{\rm pin} = 0.03$ plotted versus r on a linear scale. The upper two curves are shifted upward for clarity. (b)–(d) show the structure factors of skyrmions at $t = 20$, $t = 300$, and $t = 10000$, respectively.

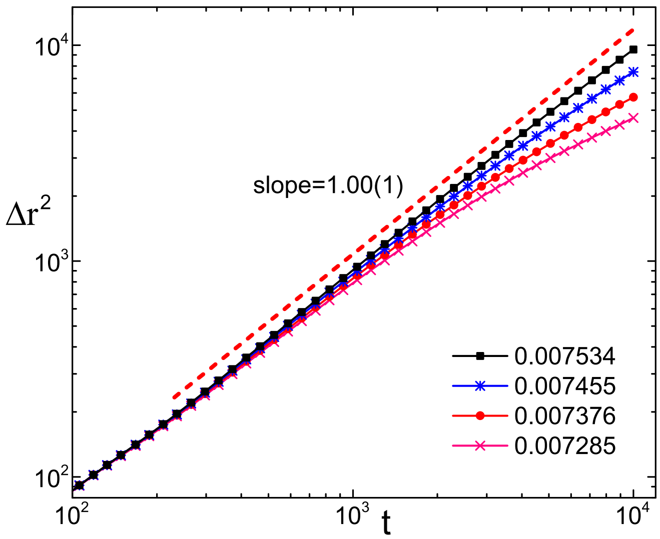

FIG. 7. The mean-square displacements versus the time t for different driving forces with $\alpha_m/\alpha_d = 9.962$ and $F_{\rm pin} = 0.03$ are plotted on a log-log scale. The dashed line shows a power-law fit for $F = 0.007534$.

In the inset, with a critical exponent $\eta_\parallel = 1.81(3)$, the data collapse of the autocorrelation function $A_\parallel(t, t_0)$ of the parallel velocity for different t_0 is demonstrated as well. The aging behavior is one of the central phenomena in the slow complex dynamics including disordered and glassy systems. The data collapse of the scaling function $F[\xi(t)/\xi(t_0)]$ reveals the temporal scale invariance, and its power-law behavior represents a long-range time correlation far from stationary.

To illustrate the structure evolution of the skyrmions with time, we plot the pair distribution function $g(r)$ and the structure factor $S(\mathbf{k}) = N_s^{-1}|\sum_{i=1}^{N_s} e^{-i\mathbf{k}\cdot\mathbf{r}_i}|$ for different times at critical force $F_c = 0.007455$ in Fig. 6. At $t = 20$, the pair distribution function still displays a long-range positional order of the skyrmions, and the structure factor indicates a hexagonal structure. However, the oscillation in the pair distribution function decays rapidly at $t = 300$, indicating that the hexagonal structure is already disordered for $t > t_{\rm mic}$. The skyrmions tend to a disordered liquidlike state at $t = 10\,000$, which can be seen in the structure factor. Finally, the skyrmions will reach a moving liquid state in the long-time limit. Simulations with other initial states, such as the disordered state and the pinned stationary state with a small driving force, lead to a similar relaxation scenario for $t > t_{\rm mic}$.

The mean-square displacement for different driving forces is displayed in Fig. 7. In the stationary state, it should asymptotically exhibit a power-law behavior, $\Delta r^2(t) \propto t^\alpha$, with α being the diffusive exponent. The dynamic relaxation in our simulations, however, is far from stationary, and $\Delta r^2(t)$ is also not the order parameter or directly relevant to it. Therefore, a power-law behavior of $\Delta r^2(t)$ is not generally observed in the time regime of our simulations. Nevertheless, as shown in Fig. 7, $\Delta r^2(t)$ presents a power-law-like behavior at $F = 0.007534$, which is just above F_c, with $\alpha \approx 1.00$, indicating that the dynamic system exhibits a regular diffusion and relaxes to a liquid state. For a smaller F, one may conceive the diffusion exponent $\alpha < 1.00$ in the long-time regime. In this subdiffusive regime, some of the skyrmions are captured by the pinning sites, and the other part undergoes dynamic fluctuations due to the interactions between skyrmions; thus, the diffusion of the skyrmions is reduced. The coordination number of this part of the skyrmions deviates from 6. Therefore, there are topological defects generated in the relaxation process, and the neighbors of the skyrmions change.

In Table I, all the critical exponents of the perpendicular and parallel directions for $\alpha_m/\alpha_d = 9.962$ at pinning strength $F_{\rm pin} = 0.03$ are summarized. The measurements of the critical exponents in the perpendicular direction are performed in the time regime starting from $t_{\rm mic} \sim 250$. The nonstationary dynamic approach to the depinning phase transition shows its very efficiency for the Magnus-dominated skyrmion motion. For the parallel direction, due to the strong correction to scaling of $\xi_\parallel(t)$, the dynamic approach should be refined by taking the spatial correlation length $\xi_\parallel(t)$ as the dynamic scaling variable. The advantage of this refined approach is that one may directly extract the static critical exponents $\beta_\parallel$ and $\nu_\parallel$, independent of possible corrections to scaling of $\xi_\parallel(t)$.

Due to the Magnus term, the skyrmions exhibit collective dynamic behaviors pronouncedly different from that of the domain wall and vortex. There exists a power-law behavior for the physical observables in the direction perpendicular to the driving force. The depinning phase transition dominated by the Magnus force of the skyrmions is of second order, in contrast to that of the vortex induced by the transverse barriers, which is of first order [44,45]. The static and dynamic universality classes of the skyrmions are obviously different from those of the domain wall [46,47] and vortex [45]. In our results, the different critical exponents of the parallel and perpendicular directions should be emphasized. For example, $\beta_\parallel = 0.96(3)$ and $\beta_\perp = 1.18(3)$ are obtained for the parallel and perpendicular directions, respectively. In Ref. [27],

TABLE I. Critical exponents of skyrmions for $\alpha_m/\alpha_d = 9.962$ at $F_{\rm pin} = 0.03$ in the perpendicular and parallel directions.

Observable	Exponent	Value	Observable	Exponent	Value
$V_\parallel(t)$	$\beta_\parallel/\nu_\parallel$	0.92(2)	$V_\perp(t)$	$\beta_\perp/\nu_\perp z_\perp$	0.77(1)
	$\beta_\parallel$	0.96(3)		$\beta_\perp$	1.18(2)
	$\nu_\parallel$	1.04(3)		$\nu_\perp$	0.85(2)
$\xi_\parallel(t)$	$z_\parallel$	1.28(3)	$\xi_\perp(t)$	$z_\perp$	1.82(3)
$A_\parallel(t, t_0)$	$\eta_\parallel$	1.81(3)	$A_\perp(t, t_0)$	$\eta_\perp$	2.79(6)
	$2 - d + 2\beta_\parallel/\nu_\parallel$	1.84(2)		$2 - d + 2\beta_\perp/\nu_\perp$	2.80(3)

TABLE II. Critical forces and critical exponents of skyrmions for different parameters in the perpendicular and parallel directions.

$F_{\rm pin}$	α_m/α_d	F_c	$\beta_\perp$	$\nu_\perp$	$z_\perp$	$\beta_\parallel$	$\nu_\parallel$	$z_\parallel$
0.03	1.000	0.009180(28)	2.00(5)	1.16(4)	2.32(7)	1.27(4)	1.11(5)	1.05(4)
	3.000	0.008746(35)	1.61(5)	1.03(3)	1.76(5)	1.13(4)	1.09(4)	1.00(4)
	5.001	0.008301(30)	1.35(3)	0.91(2)	1.78(4)	1.08(3)	1.06(3)	1.17(3)
	7.498	0.007827(28)	1.19(3)	0.87(2)	1.79(4)	0.97(3)	1.05(3)	1.23(4)
	9.962	0.007455(25)	1.18(2)	0.85(2)	1.82(3)	0.96(3)	1.04(3)	1.28(3)
0.05	9.962	0.01381(30)	0.95(3)	1.38(4)	0.99(3)	0.83(3)	1.06(4)	1.16(4)

a critical exponent β was briefly estimated from the ratio $R = |V_\perp/V_\parallel|$, ranging from $\beta = 0.15$ to $\beta = 0.5$ for different α_m/α_d. This critical exponent β should be compared with our result $\beta_\perp - \beta_\parallel = 0.22(3)$. Since there is a strong correction to the power-law behavior of $V_\parallel$, the ratio R does not present a power-law behavior at the critical force in our simulations. This implies that R may not be a suitable order parameter in the skyrmion depinning phase transition.

A recent experiment suggested that the skyrmion Hall angle $\theta_{sk} = \tan^{-1}(R)$ depends on the driving force in the presence of defects around the critical force [15]. This may be understood from the different critical behaviors in the directions perpendicular and parallel to the driving force at the depinning phase transition. Near the depinning phase transition, the velocity obeys a power-law behavior $V \sim (F - F_c)^\beta$. For the typical parameters $\alpha_m/\alpha_d = 9.962$ and $F_{\rm pin} = 0.03$ [14], the numerical result $\beta_\parallel = 0.96(3)$ indicates that $V_\parallel$ increases almost linearly with the driving force. But $\beta_\perp = 1.18(3)$ shows a nonlinear dependence of $V_\perp$. It reveals that the nonlinear response of the skyrmion Hall angle may be mainly due to the perpendicular motion induced by the Magnus term.

In numerical simulations of two-dimensional periodic magnetic systems, however, various critical exponents have been obtained. $\beta = 0.29(3)$ and $\beta = 1.3(1)$ are for the elastic and plastic depinning transitions of vortices [29,48], and $\beta = 0.59(1)$ is for the domain wall of the Heisenberg model [35]. The static exponent $\nu_\parallel = 1.04(3)$ for the skyrmions happens to be the same as that of the domain wall within errors, but $\nu_\perp = 0.85(2)$ is rather distinct from that of the domain wall and vortex [32,35]. Based on the standard scaling analysis for second-order phase transitions, one may obtain a hyperscaling relation for the critical exponent, $\eta = 2 - d + 2\beta/\nu$, with $d = 2$ being the spatial dimension of the skyrmion system. In our simulations, the direct measurements of $\eta_\perp = 2.79(6)$ and $\eta_\parallel = 1.81(3)$ from the aging behavior agree well with the results $\eta_\perp = 2.80(3)$ and $\eta_\parallel = 1.84(2)$, respectively, predicted by the scaling relation with $\beta_\perp/\nu_\perp = 1.40(2)$ and $\beta_\parallel/\nu_\parallel = 0.92(2)$ as input, which are measured from the power-law behavior of the velocities.

For a more comprehensive understanding of the depinning phase transition of skyrmions, we have performed simulations for different Magnus forces and pinning forces, and the results are listed in Table II. The critical force is reduced when the magnitude of the Magnus force increases, which is consistent with the results of Ref. [14]. For the pinning force $F_{\rm pin} = 0.03$, all the static exponents $\beta_\perp$ and $\nu_\perp$ and $\beta_\parallel$ and $\nu_\parallel$ decrease with increasing α_m/α_d and become robust at the larger α_m/α_d limit. If the strength α_m/α_d of the Magnus term is reduced to zero, the exponent $\beta_\parallel$ tends to that of vortices, $\beta = 1.3(1)$. In other words, there is a crossover from the universal class from the damping-dominated system to the Magnus-dominated system when the Magnus force increases. For a stronger disorder strength $F_{\rm pin} = 0.05$, all the critical exponents are different from those of $F_{\rm pin} = 0.03$, especially in the perpendicular direction. In general, the critical exponents β, ν, and z are different in the directions perpendicular and parallel to the driving force, and the anisotropic critical behaviors exist in various regions of the parameter space.

The Magnus term induces a spiraling motion when the skyrmion enters a pinning site [22,23]. This is in contrast to the overdamped particles, such as vortices, which simply travel directly to the bottom of the pinning potential; thus, the Magnus term may lead to a new universal class of the depinning phase transitions. Further, due to the Magnus term, a moving skyrmion exhibits a side jump phenomenon in the direction of the driving force in the presence of disorder, and dynamic behaviors in the perpendicular and parallel directions are different [49]. These peculiarities give rise to the novel dynamic features of skyrmions at the depinning phase transition.

V. CONCLUSION

We investigated the nonstationary dynamic behaviors of skyrmions in two-dimensional magnetic materials with quenched defects based on the Thiele equation of the particle model. The critical force was convincingly located by the power-law behavior of the velocity, and its value is supportive of and more precise than that in the experiment with MnSi. The static and dynamic exponents were then accurately determined for different strengths of the Magnus term and the pinning force. Importantly, the critical dynamics of the Magnus-dominated topological skyrmions demonstrates different collective transport properties in the directions perpendicular and parallel to the driving force, and the anisotropy exists in various regions of the parameter space. This anisotropic character provides an understanding of the force-dependent skyrmion Hall angle in the experiment and guidance for the effective manipulation and the precise measurement of the Hall effect of skyrmions in a magnetic thin film with disorder. The Magnus interaction induces a distinct dynamic behavior of skyrmions which is in a different universality class of the depinning phase transitions compared to other overdamped magnetic systems, such as the vortices and domain walls. The critical exponents of skyrmions are significantly different from those of the vortices and domain walls. Especially, the difference of β is over 30% in the driving direction when the strength α_m/α_d of the Magnus term is large. Our nonstationary dynamic approach to the molecular dynamics simulation is very efficient and could be extended to dynamic simulations of various magnetic systems.

ACKNOWLEDGMENTS

This work was supported in part by the National Natural Science Foundation of China under Grants No. 11775186, No. 11375149, and No. 11875120 and the Zhejiang Provincial Natural Science Foundation under Grant No. LY17A050002.

[1] T. H. R. Skyrme, Proc. R. Soc. London, Ser. A **260**, 127 (1961).
[2] X. Z. Yu, Y. Onose, N. Kanazawa, J. H. Park, J. H. Han, Y. Matsui, N. Nagaosa, and Y. Tokura, Nature (London) **465**, 901 (2010).
[3] S. A. Montoya, R. Tolley, I. Gilbert, S.-G. Je, M.-Y. Im, and E. E. Fullerton, Phys. Rev. B **98**, 104432 (2018).
[4] S. Heinze, K. von Bergmann, M. Menzel, J. Brede, A. Kubetzka, R. Wiesendanger, G. Bihlmayer, and S. Blügel, Nat. Phys. **7**, 713 (2011).
[5] S. Woo, K. Litzius, B. Krüger, M.-Y. Im, L. Caretta, K. Richter, M. Mann, A. Krone, R. M. Reeve, M. Weigand, P. Agrawal, I. Lemesh, M.-A. Mawass, P. Fischer, M. Kläui, and G. S. D. Beach, Nat. Mater. **15**, 501 (2016).
[6] J. Zang, M. Mostovoy, J. H. Han, and N. Nagaosa, Phys. Rev. Lett. **107**, 136804 (2011).
[7] X. Z. Yu, N. Kanazawa, W. Z. Zhang, T. Nagai, T. Hara, K. Kimoto, Y. Matsui, Y. Onose, and Y. Tokura, Nat. Commun. **3**, 988 (2012).
[8] X. Z. Yu, N. Kanazawa, Y. Onose, K. Kimoto, W. Z. Zhang, S. Ishiwata, Y. Matsui, and Y. Tokura, Nat. Mater. **10**, 106 (2010).
[9] N. Romming, C. Hanneken, M. Menzel, J. E. Bickel, B. Wolter, K. von Bergmann, A. Kubetzka, and R. Wiesendanger, Science **341**, 636 (2013).
[10] T. Schulz, R. Ritz, A. Bauer, M. Halder, M. Wagner, C. Franz, C. Pfleiderer, K. Everschor, M. Garst, and A. Rosch, Nat. Phys. **8**, 301 (2012).
[11] F. Jonietz, S. Mühlbauer, C. Pfleiderer, A. Neubauer, W. Münzer, A. Bauer, T. Adams, R. Georgii, P. Böni, R. A. Duine, K. Everschor, M. Garst, and A. Rosch, Science **330**, 1648 (2010).
[12] J. Iwasaki, M. Mochizuki, and N. Nagaosa, Nat. Commun. **4**, 1463 (2013).
[13] N. Nagaosa and Y. Tokura, Nat. Nanotechnol. **8**, 899 (2013).
[14] C. Reichhardt, D. Ray, and C. J. O. Reichhardt, Phys. Rev. Lett. **114**, 217202 (2015).
[15] W. Jiang, X. Zhang, G. Yu, W. Zhang, X. Wang, M. B. Jungfleisch, J. Pearson, X. Cheng, O. Heinonen, K. L. Wang, Y. Zhou, A. Hoffmann, and S. G. E. te Velthuis, Nat. Phys. **13**, 162 (2016).
[16] C. Hanneken, A. Kubetzka, K. von Bergmann, and R. Wiesendanger, New J. Phys. **18**, 055009 (2016).
[17] S. Woo, K. M. Song, H.-S. Han, M.-S. Jung, M.-Y. Im, K.-S. Lee, K. S. Song, P. Fischer, J.-I. Hong, J. W. Choi, B.-C. Min, H. C. Koo, and J. Chang, Nat. Commun. **8**, 15573 (2017).
[18] J.-V. Kim and M.-W. Yoo, Appl. Phys. Lett. **110**, 132404 (2017).
[19] C. Reichhardt, D. Ray, and C. J. O. Reichhardt, Phys. Rev. B **98**, 134418 (2018).
[20] S. Hoshino and N. Nagaosa, Phys. Rev. B **97**, 024413 (2018).
[21] A. A. Thiele, Phys. Rev. Lett. **30**, 230 (1973).
[22] S.-Z. Lin, C. Reichhardt, C. D. Batista, and A. Saxena, Phys. Rev. B **87**, 214419 (2013).
[23] Y.-H. Liu and Y.-Q. Li, J. Phys.: Condens. Matter **25**, 076005 (2013).
[24] S. D. Yi, S. Onoda, N. Nagaosa, and J. H. Han, Phys. Rev. B **80**, 054416 (2009).
[25] S. Woo, K. M. Song, X. Zhang, Y. Zhou, M. Ezawa, X. Liu, S. Finizio, J. Raabe, N. J. Lee, S.-I. Kim, S.-Y. Park, Y. Kim, J.-Y. Kim, D. Lee, O. Lee, J. W. Choi, B.-C. Min, H. C. Koo, and J. Chang, Nat. Commun. **9**, 959 (2018).
[26] K. Litzius, I. Lemesh, B. Krüger, P. Bassirian, L. Caretta, K. Richter, F. Büttner, K. Sato, O. A. Tretiakov, J. Förster, R. M. Reeve, M. Weigand, I. Bykova, H. Stoll, G. Schütz, G. S. D. Beach, and M. Kläui, Nat. Phys. **13**, 170 (2016).
[27] C. Reichhardt and C. J. O. Reichhardt, New J. Phys. **18**, 095005 (2016).
[28] C. J. Olson, C. Reichhardt, and V. M. Vinokur, Phys. Rev. B **64**, 140502(R) (2001).
[29] Y. Fily, E. Olive, N. Di Scala, and J. C. Soret, Phys. Rev. B **82**, 134519 (2010).
[30] W.-P. Cao, M.-B. Luo, and X. Hu, New J. Phys. **14**, 013006 (2012).
[31] M. J. P. Gingras and D. A. Huse, Phys. Rev. B **53**, 15193 (1996).
[32] Y. Kawamura, S. Moriya, K. Ienaga, S. Kaneko, and S. Okuma, New J. Phys. **19**, 093001 (2017).
[33] M. H. Jin, B. Zheng, L. Xiong, N. J. Zhou, and L. Wang, Phys. Rev. E **98**, 022126 (2018).
[34] S. A. Díaz, C. J. O. Reichhardt, D. P. Arovas, A. Saxena, and C. Reichhardt, Phys. Rev. B **96**, 085106 (2017).
[35] L. Xiong, B. Zheng, M. H. Jin, L. Wang, and N. J. Zhou, New J. Phys. **20**, 023027 (2018).
[36] E. V. Albano, M. A. Bab, G. Baglietto, R. A. Borzi, T. S. Grigera, E. S. Loscar, D. E. Rodriguez, M. L. R. Puzzo, and G. P. Saracco, Rep. Prog. Phys. **74**, 026501 (2011).
[37] B. Zheng, Int. J. Mod. Phys. B **12**, 1419 (1998).
[38] B. Zheng, M. Schulz, and S. Trimper, Phys. Rev. Lett. **82**, 1891 (1999).
[39] X. W. Lei and B. Zheng, Phys. Rev. E **75**, 040104(R) (2007).
[40] A. B. Kolton, G. Schehr, and P. Le Doussal, Phys. Rev. Lett. **103**, 160602 (2009).
[41] C. Reichhardt and C. J. O. Reichhardt, Rep. Prog. Phys. **80**, 026501 (2017).
[42] S. Z. Lin, B. Zheng, and S. Trimper, Phys. Rev. E **73**, 066106 (2006).
[43] Y. Yang, D. McDermott, C. J. O. Reichhardt, and C. Reichhardt, Phys. Rev. E **95**, 042902 (2017).

[44] C. J. Olson and C. Reichhardt, Phys. Rev. B **61**, R3811 (2000).
[45] T. Nattermann and S. Scheidl, Adv. Phys. **49**, 607 (2000).
[46] N. J. Zhou, B. Zheng, and Y. Y. He, Phys. Rev. B **80**, 134425 (2009).
[47] Y. Y. He, B. Zheng, and N. J. Zhou, Phys. Rev. B **94**, 134302 (2016).
[48] N. D. Scala, E. Olive, Y. Lansac, Y. Fily, and J. C. Soret, New J. Phys. **14**, 123027 (2012).
[49] J. Müller and A. Rosch, Phys. Rev. B **91**, 054410 (2015).